Am J Physiol Heart Circ Physiol. Author manuscript; available in PMC 2013 June 28.

Published in final edited form as:

Am J Physiol Heart Circ Physiol. 2012 March 15; 302(6): H1330–H1339. doi:10.1152/ajpheart.01044.2011.

Catechin prevents severe dyslipidemia-associated changes in wall biomechanics of cerebral arteries in LDLr$^{-/-}$:hApoB$^{+/+}$ mice and improves cerebral blood flow

Virginie Bolduc[1,4], **Edward Baraghis**[4,5], **Natacha Duquette**[4], **Nathalie Thorin-Trescases**[4], **Jean Lambert**[2], **Frédéric Lesage**[4,5], and **Eric Thorin**[3,4]

[1]Université de Montréal, Faculty of Medicine, Department of Pharmacology, Montreal, Quebec, Canada

[2]Université de Montréal, Faculty of Medicine, Department of Social and Preventive Medicine, Montreal, Quebec, Canada

[3]Université de Montréal, Faculty of Medicine, Department of Surgery, Montreal, Quebec, Canada

[4]Montreal Heart Institute Research Center, Montreal, Quebec, Canada

[5]École Polytechnique de Montréal, Montreal, Quebec, Canada

Abstract

Endothelial dysfunction and oxidative stress contribute to the atherosclerotic process that includes stiffening of large peripheral arteries. In contrast, our laboratory previously reported a paradoxical increase in cerebro-vascular compliance in LDLr$^{-/-}$:hApoB$^{+/+}$ atherosclerotic (ATX) mice (7). We hypothesized that prevention of cerebral artery endothelial dysfunction with a chronic dietary antioxidant intake would normalize the changes in cerebral artery wall structure and biomechanics and prevent the decline in basal cerebral blood flow associated with atherosclerosis. Three-month-old ATX mice were treated, or not, for 3 mo with the polyphenol (+)-catechin (CAT; 30 mg·kg^{-1}·day^{-1}) and compared with wild-type controls. In isolated, pressurized cerebral arteries from ATX mice, CAT prevented endothelial dysfunction (deterioration of endothelium-dependent, flow-mediated dilations; $P < 0.05$), the inward hypertrophic structural remodeling (increase in the wall-to-lumen ratio; $P < 0.05$), and the rise in cerebrovascular compliance (rightward shift of the stress-strain curve measured in passive conditions, reflecting mechanical properties of the arterial wall; $P < 0.05$). Doppler optical coherence tomography imaging in vivo confirmed these findings, showing that cerebral compliance was higher in ATX mice and normalized by CAT ($P < 0.05$). CAT also prevented basal cerebral hypoperfusion in ATX mice ($P < 0.05$). Active remodeling of the cerebrovascular wall in ATX mice was further suggested by the increase ($P < 0.05$) in pro-

Address for reprint requests and other correspondence: E. Thorin, Montreal Heart Institute, Research Center, 5000 rue Bélanger, Montreal, QC, Canada H1T 1C8 (eric.thorin@umontreal.ca).

DISCLOSURES

No conflicts of interest, financial or otherwise, are declared by the author(s).

AUTHOR CONTRIBUTIONS

V.B. and E.T. conception and design of research; V.B., E.B., N.D., and F.L. performed experiments; V.B., E.B., N.T.-T., J.L., F.L., and E.T. analyzed data; V.B., N.T.-T., F.L., and E.T. interpreted results of experiments; V.B. and N.T.-T. prepared figures; V.B. and N.T.-T. drafted manuscript; V.B., E.B., N.T.-T., F.L., and E.T. edited and revised manuscript; V.B., E.B., N.D., N.T.-T., J.L., F.L., and E.T. approved final version of manuscript.

metalloproteinase-9 activity, which was normalized by CAT. We conclude that, by preserving the endothelial function, a chronic treatment with CAT prevents the deleterious effect of severe dyslipidemia on cerebral artery wall structure and biomechanical properties, contributing to preserving resting cerebral blood flow.

Keywords

polyphenol; optical coherence tomography; pressurized arteries; cerebrovascular compliance; wall remodeling

Atherosclerosis is associated with endothelial dysfunction (11, 16), an increased production of reactive oxygen species (ROS) (21), and changes in the compliance and structure of large elastic peripheral and small cerebral arteries (7, 46), and it is a major risk factor for stroke (47). The term compliance refers to the changes in volume contained within an artery for a given change in transmural pressure and reflects the degree of arterial elasticity. The term capacitance, also used in this context, specifically refers to the volume of blood in the vessel wall, for a given pressure. Thus highly distensible vessels display a higher compliance/capacitance than stiff vessels. Our laboratory previously reported that, in severely dyslipidemic, spontaneously atherosclerotic (ATX) LDLr$^{-/-}$:hApoB$^{+/+}$ mice, which develop lesions in large peripheral arteries (aorta, renal, and carotid arteries), are hypertensive, and exhibit cerebral hypoperfusion and cognitive decline (7, 11, 16), cerebral and carotid arteries display opposite changes in vascular compliance in vitro (7) and in vivo (4); while, as expected, carotid arteries stiffen, cerebrovascular compliance increases with atherosclerosis. Our laboratory recently proposed that the compliance of cerebral arteries is dependent on the endothelial function (7), while that of the carotids is more influenced by the mechanical stress imposed to the wall by the cardiac cycle, as it has been suggested by others (1, 7, 17, 30). These conclusions were indirectly validated through the use of three experimental approaches: *1*) ivabradine that reduces heart rate (HR) and thus mechanical stress, maintained endothelial function and cerebrovascular compliance; *2*) metoprolol worsened cerebral endothelial function and the compliance; and *3*) exposure to physical training normalized the endothelial function and cerebrovascular compliance, without reducing mechanical stress (7). Endothelial function and cerebral compliance seem, therefore, tightly associated.

Another way to protect the endothelium is the use of anti-oxidants. The efficiency of antioxidant therapy to reduce the progression of an evolving lesion in the aorta, to lower proinflammatory mediators, to reverse endothelial dysfunction, and to reduce ROS accumulation in the vasculature has been demonstrated in animal models (9, 16, 27, 52). These mouse models of atherosclerosis (i.e., ApoE$^{-/-}$ and LDLr$^{-/-}$:hApoB$^{+/+}$) rarely develop lesions in the cerebral vasculature before the age of 6 mo; however, the benefits of antioxidants clearly extended to the brain and cerebral arteries function (11): our laboratory reported that catechin (CAT), a polyphenol with antioxidant properties and member of the flavonoid family (48), significantly preserved flow-mediated dilations (FMD) of cerebral resistance arteries and improved cerebral blood flow (CBF) responses to neuronal stimulations and cognitive functions in ATX mice (11). It is not known, however, if CAT

restores the structural changes leading to an increased compliance of cerebral arteries. These biomechanical alterations could contribute, in addition to the endothelial dysfunction and the higher myogenic responses, to the decreased capacity of the brain to autoregulate its perfusion. To the best of our knowledge, the effects of CAT on the structure of the cerebral arteries in mice with severe dyslipidemia and developing atherosclerotic lesions in conductance arteries have not been reported. The objective of this study was to demonstrate that, by improving cerebrovascular endothelial function, CAT prevents adverse wall remodeling; we hypothesized that this would contribute to maintain basal CBF. Accordingly, we found not only that CAT prevents the remodeling of cerebral resistance arteries occurring in LDLr$^{-/-}$:hApoB$^{+/+}$ mice, but it also normalizes the cerebrovascular compliance, measured ex vivo in passive conditions, as well as in vivo, and improves basal CBF. These combined beneficial effects could, therefore, contribute to the protective effects of CAT on basal CBF regulation previously reported with polyphenols (11, 44, 45).

MATERIALS AND METHODS

The procedures and protocols were approved by our institutional animal ethical committee and performed with the Guide for the Care and Use of Laboratory Animals of Canada and the Guide for the Care and Use of Laboratory Animals published by the US National Institutes of Health (National Institutes of Health Publication No. 85–23, revised 1996).

Experiments were conducted on posterior cerebral arteries (PCA) isolated from 6-mo-old (mo) male C57BL/6 wild type (WT) (n = 15) (Charles River Laboratories, St-Constant, QC, Canada) used as controls, and from 6-mo male ATX mice (LDLr$^{-/-}$:hApoB-100$^{+/+}$) (n = 27) (11, 16, 41). ATX mice were randomly assigned to receive, or not (n = 17), a 3-mo (from 3- to 6-mo) (+)-catechin hydrate (Sigma-Aldrich Canada, Oakville, Ontario, Canada) treatment (ATX+CAT; 30 mg·kg^{-1}·day^{-1}; n = 10) (11) in the drinking water. At 6 mo, mice were anesthetized (44 mg/kg ketamine, 2.2 mg/kg xylazine) and blood was collected; the plasma was frozen at −80°C. The brain was removed from the cranial cavity and frozen at −80°C, or placed in ice-cold physiological salt solution (PSS) for reactivity and compliance studies. The carotid arteries were removed and placed in ice-cold PSS for compliance studies.

Plasma parameters

Total cholesterol, low-density lipoproteins, high-density lipoproteins, triglycerides, and glucose levels were measured at the Montreal Heart Institute clinical biochemistry laboratory (Montreal, QC, Canada). VEGF level was quantified with the Fluorokine MAP Mouse VEGF Kit (R&D Systems, Minneapolis, MN).

Tail cuff

For n = 6 –9 mice in each group (WT, ATX, and ATX+CAT mice), HR and blood pressure were monitored weekly from 3 to 6 mo by tail-cuff plethysmography (Kent Scientific, Torrington, CT). Mice were inserted in a holder on a heated platform 15 min before pressure measurements. When the tail reached 30°C, 30 recordings were collected. Mice were trained for five sessions 3 wk before (baseline) starting the weekly recording at 3 mo.

Reactivity studies

PCA were isolated, cannulated at both ends, and pressurized, as previously described (13). The media used for the isolated vessels was PSS (pH 7.4, mmol/l: 130 NaCl, 4.7 KCl, 1.18 KH_2PO_4, 1.17 $MgSO_4$, 14.9 $NaHCO_3$, 1.6 $CaCl_2$, 0.023 EDTA, and 10 glucose) aerated with 12% O_2/5% CO_2/83% N_2. FMD were induced on phenylephrine (10 μM) (Sigma-Aldrich Canada, Oakville, Ontario, Canada) preconstricted arteries (13). Arteries were perfused with PSS. A single cumulative curve (from 0 to 20 dyn/cm^2, with 2 dyn/cm^2 steps between 0 and 10 dyn/cm^2, followed by two 5 dyn/cm^2 steps, at constant pressure of 60 mmHg) was performed on each segment (7). The flow rate through the lumen (Q) (ml/s) required to match a given shear stress value (τ, dyn/cm^2) was calculated for each point on the curve according to [$Q = (\tau\pi r^3)/4\eta$], where η represents the viscosity (0.009 Poise), and r the inside radius (cm). The applied calculated shear stress was in the physiological range (≈ 0 –25 dyn/cm^2) (31, 36). The data are presented as the percentage of dilation for every shear stress value.

Measurements of ex vivo cerebral arteries biomechanics and structure

PCA and carotid arteries were used for the in vitro assessment of the compliance, measured in passive conditions to reflect mechanical properties of the vascular wall. Passive pressure-diameter curves were conducted in a Ca^{2+}-free PSS containing 1 mM of EGTA and 10 μM of sodium nitroprusside to abolish myogenic tone and to solely assess the mechanical properties of the arteries. Lumen diameter and outer diameter changes were measured after each increment in the intraluminal pressure (from 10 to 120 mmHg, with a first 10-mmHg step followed by 20-mmHg steps for PCA and from 60 to 180 mmHg with 20-mmHg steps for carotid arteries) to calculate the structural and mechanical parameters of the arterial wall. The wall thickness (μm) was calculated according to [(external diameter – lumen diameter)/2] for the values obtained at 10 mmHg. The wall-to-lumen ratio was calculated according to wall thickness/lumen diameter for the values obtained at 10 mmHg. For the structural parameters (lumen diameter, wall thickness, and wall-to-lumen ratio), the values are only presented at 10 mmHg to eliminate the effect of distensibility, but in noncollapsed vessels. The circumferential wall strain (strain, %) was calculated according to [$(D - D_{10\ mmHg})/D_{10\ mmHg}$], where D is the internal diameter at a given pressure, and $D_{10\ mmHg}$ is the initial diameter at the initial pressure. The circumferential wall stress (stress, dyn/cm^2) was calculated according to [(P × 1,334 × D)/2 × wall thickness], where P is the given intraluminal pressure (1 mmHg = 1,334 dyn/cm^2). The stress-strain relationship was calculated by fitting the data to a nonlinear exponential curve ($\mathrm{stress}=\mathrm{stress}_0^{\beta\mathrm{strain}}$), where stress_0 is the value when strain equals 0, and β is a constant representing Young's elastic modulus.

The incremental distensibility (ID; %/mmHg), which represents the percentage of change of the arterial internal diameter for each millimeters of mercury change in intraluminal pressure, was calculated according to [$(D_1 - D_0)/(D_1 \times \Delta P) \times 100$], where D_0 is the internal diameter before the pressure increment, D_1 is the internal diameter after the pressure increment, and ΔP is the change in intraluminal pressure (10 or 20 mmHg).

In vivo estimation of cerebrovascular compliance and basal cerebral blood

Compliance and basal CBF of small brain arteries located in the somatory-sensory cortex, a region supplied by the middle cerebral artery (MCA) and its branches, were measured in vivo using a Doppler optical coherence tomography system previously described (4, 11). Our gold standard consisted in controlled measures of viscous flow in phantoms (4). Acquisitions were made to quantitatively assess basal CBF over the cardiac cycle. The system used is based on a superluminescent diode emitting near infrared light at 870 nm with a bandwidth of 65 nm. Light on the sample was 2.5 mW, yielding a sensitivity of 106 dB with a dynamic range of 76 dB. Acquisition was done at a frequency of ~15 kHz, which gives a maximum detectable Doppler speed of 3 mm/s. Lateral and axial resolutions were 10 and 7 μm, respectively. At 6 mo, mice were anesthetized (2 g/kg, urethane), and a tracheotomy was performed. The mice were placed in a stereotaxic stage, and the skin on the top of the scalp was removed to image the somatosensory cortex with a ×10 water microscope objective. Body temperature was kept at 37°C with a heating pad until the experiment was completed. HR was monitored during the experiment, but neither blood pressure nor blood gases were recorded. Acquisitions were done on a 800-μm by 800-μm field of view; the depth of penetration allowed imaging of structures up to 600 μm beneath the surface. We calculated the absolute CBF (nl/s) as previously described (11) in the imaged arteries and all of its visible collateral branches, normalized by the cross-sectional area (mm^2). CBF values were compared between WT, ATX, and CAT-treated ATX mice, in animals with similar HRs (409 ± 10, 423 ± 10, and 438 ± 7 beats/min, respectively) during acquisitions. CBF was measured in a region supplied by the MCA, while arterial function/structure was assessed in the PCA, but both arteries derive from the internal carotid and form an independent domain in the circle of Willis of the mouse brain (35).

For compliance, imaged arteries with similar diameter were found at the interface between the skull and the brain at a depth of ~400 μm. Image reconstruction yielded a quantitative average value of blood flow (Q_{Av}, m^3/s) and a vascular cross-sectional area (A_{Av}, m^2). The cardiac profile of the vessel flow was determined using an ECG gated reconstruction technique. Change in blood speed [δ_v; arbitrary units (AU)] and in vessel area (δ_A; AU) between diastole and systole was obtained from this profile. The blood viscosity (η; cP) was calculated for each vessel using the vessel diameter and hematocrit calculated according to a previously described formula (40). A local compliance evaluator (nl/Pa) can be obtained with:

$$\text{Compliance}=\{[(A_{\text{Av}})^3/Q_{\text{Av}}]\times[(\delta_A+1)\times\delta_A/\delta_v]\times 10^{15}\}/\eta$$

Isolation of cerebral vessels and Western blot

Whole brain vessels were isolated as previously described (26). For Western blot analysis, 30 μg of cerebral vessels proteins were mixed with a discontinuous Laemmli buffer and loaded on a 10% acrylamide SDS-PAGE gels. After 45 min of migration at 200 V, gels were transferred on nitrocellulose. Membranes were incubated with an anti-VEGF (1: 1,000, Abcam, Cambridge, MA). α-Actin was used as a loading control (anti-α-actin 1:100 000,

Sigma-Aldrich Canada, Oakville, Ontario, Canada). Quantification was made by densitometric analysis using Quantity One software.

Gelatin zymography

Zymography using gelatin-containing gels was performed as described previously (23). Briefly, a modified Laemmli buffer without mercaptoethanol was added to the vessel proteins samples, without heating, on a 6% SDS-polyacrylamide gel containing 1% gelatin. Migration was conducted at 4°C and 20 mA for 1 h, followed by a migration (90 V) for 2 h. After migration, SDS was removed from the gel by washing 5 × 10 min with 2.5% (vol/vol) Triton X-100 at room temperature. Gels were incubated in a zymography buffer (38 mM Tris·HCl, pH 7.4, 13 mM $CaCl_2$, 10 μM $ZnCl_2$, 0.02% NaN_3, and 0.03% Brij 35) at 37°C for 72 h and then stained with Coomassie brilliant blue. Gelatinolytic activity was visualized as clear bands against the dark background. Samples of purified human pro-matrix metalloproteinase (MMP)-9 (Chemicon International) and pro-MMP-2 (Enzo Life Sciences, Plymouth Meeting PA) were used as positive controls. Quantification was made by densitometric analysis using Gimp 2.6 software. To test if CAT could directly inhibit MMP-9, we incubated gels in a zymographic buffer containing 3.1 μM CAT. This concentration represents the approximate CAT absorption per day and per mouse if the absorption rate were equal to 100%.

Statistics

"*n*" refers to the number of animals used in each protocol. Results are presented as means ± SE. Unpaired Student's *t*-test and one-way ANOVA were used, when adequate. A value of $P < 0.05$ was considered statistically significant. Statistical analyses were mostly performed with GraphPad Prism 5 (GraphPad Software, La Jolla, CA). Statistical analyses of basal CBF were performed with SPSS 19.0 (SPSS, Chicago, IL): 191 measurements of basal CBF were obtained from 10 mice in which similar HR was simultaneously recorded; therefore, the parameter CBF was analyzed using generalized estimating equations to take into account correlated data. The CBF was positively skewed, so inverse Gaussian and gamma distributions were tested with different link functions [identity, log, power (−2)]. Two working correlation structures were also tested: exchangeable and unstructured. The goodness of fit quasi-likelihood under independence criterion was used to compare the choices of distributions, link functions, and working correlation structures. The best results were obtained with the inverse Gaussian distribution, the log link function, and the exchangeable correlation structure. For each group of mice, CBF marginal means were estimated and compared with pairwise contrasts using the Sidak approach for adjusting the significance level. This method provides tighter bounds than the Bonferroni approach.

RESULTS

Phenotype of WT and ATX mice

The body weight was similar in WT and ATX mice and was not affected by CAT treatment (Table 1). Nonfasting plasma lipids were higher in ATX compared with WT mice, while glucose was lower (Table 1). CAT further increased plasma levels of total cholesterol and low-density lipoprotein-cholesterol, but did not affect those of glucose (Table 1). Blood

pressures assessed by tail-cuff were higher in 6-mo ATX compared with age-matched WT mice, while pulse pressure and HR were similar between both groups (Table 2). CAT affected significantly neither blood pressure, pulse pressure, nor HR in conscious mice (Table 2).

Carotid artery compliance

Compared with 6-mo WT mice, carotid arteries from 6-mo ATX mice were less compliant, as illustrated by a leftward shift of the passive stress-strain curve and a trend for a lower ID between 100 and 120 mmHg (Fig. 1, *A* and *C*). The calculated values of Young's elastic modulus in ATX mice, however, were not significantly different compared with those calculated in WT mice ($\beta = 39 \pm 9 \times 10^{-3}$ vs. $44 \pm 6 \times 10^{-3}$, ATX vs. WT mice). CAT did not prevent carotid stiffness associated with severe dyslipidemia (Fig. 1, *A* and *C*).

Cerebral artery structure, compliance, and endothelial function

In contrast to carotid arteries, cerebrovascular compliance increased in ATX mice, as shown by a rightward shift of the passive stress-strain curve (Fig. 1*B*) and by a lower value of Young's elastic modulus compared with WT mice ($\beta = 40 \pm 2 \times 10^{-3}$ vs. $60 \pm 2 \times 10^{-3}$, ATX vs. WT mice, $P < 0.05$). ID was also higher in ATX mice between 20 – 40 and 60 – 80 mmHg compared with WT mice (Fig. 1*D*). CAT fully normalized the increase in cerebrovascular compliance associated with severe dyslipidemia: it prevented the shift of the passive stress-strain curve (Fig. 1*B*) and the decrease of Young's elastic modulus ($\beta = 50 \pm 2 \times 10^{-3}$ vs. $60 \pm 2 \times 10^{-3}$, ATX+CAT vs. ATX mice, $P < 0.05$). This was attributable to a significant decrease of ID between 10 –20 and 40 – 60 mmHg (Fig. 1*D*). Interestingly, at low pressures (10 –20 mmHg), cerebral arteries isolated from ATX+CAT mice were even less distensible than those from WT mice (Fig. 1*D*).

We studied the structural properties of the PCA by ex vivo measurement of the internal and external diameter in passive conditions at 10 mmHg. PCA from ATX mice exhibited a hypertrophic inward remodeling suggested by a decreased lumen diameter and a thickening of the vessel wall, leading to an increased wall-to-lumen ratio compared with arteries from WT mice (Fig. 2, *A*, *C*, and *D*). External diameters did not change among groups (Fig. 2*B*). CAT prevented this adverse wall remodeling (Fig. 2, *A* and *D*). Accordingly, the calculated cross-sectional areas were higher in cerebral arteries from ATX mice ($7{,}007 \pm 373\ \mu m^2$, $n = 17$) than from WT mice ($5{,}910 \pm 337\ \mu m^2$, $n = 15$, $P < 0.05$), and this tended to be prevented by CAT ($6{,}640 \pm 441\ \mu m^2$, $n = 10$) (data not shown).

Endothelium-dependent FMD were significantly reduced in cerebral arteries from ATX mice from 4 to 20 dyn/cm^2, compared with FMD observed in WT mice (Fig. 3). CAT improved endothelial function at low and moderate physiological values of shear stress (31) (between 6 –10 dyn/cm^2) compared with untreated-ATX mice (Fig. 3). In CAT-treated mice, however, the FMD curve is biphasic, suggesting that the protective effect of CAT could be lost for shear stresses > 10 dyn/cm^2 (Fig. 3).

Neither contractile nor dilatory properties of the smooth muscle were affected by atherosclerosis and/or CAT treatment: phenylephrine or potassium-induced contractions were very similar in WT, ATX, and ATX+CAT mice (data not shown). In addition, sodium

nitroprusside induced identical endothelium-independent dilations in WT and ATX mice, with similar sensitivity (pD_2 in WT: 6.91 ± 0.19, in ATX: 6.82 ± 0.08) and efficacy (E_{max} in WT: 81 ± 3%, in ATX: 74 ± 6%). These data indicate that, in contrast to the endothelial function, vascular smooth muscle contractile properties are unlikely affected by atherosclerosis and/or CAT.

In vivo estimation of cerebrovascular compliance and basal cerebral blood

Using the Doppler optical coherence tomography imaging system, the local compliance evaluator was estimated for intracranial arteries of similar diameter (WT: 94 ± 5 μm, $n = 10$ mice; ATX: 107 ± 12, $n = 10$ mice; ATX+CAT: 80 ± 5, $n = 4$ mice; the measurement was performed in 2 to 5 vessels per mouse). In agreement with the data collected ex vivo, the local in vivo cerebral compliance evaluator was higher in ATX than in WT mice ($P < 0.05$) and was normalized by CAT ($P < 0.05$) (Fig. 4*A*). We measured simultaneously basal CBF (nl/s) in the selected arteries and all visible collateral branches (diameters were ranging from 21 to 279 μm, WT: 67 ± 3 μm, $n = 161$; ATX: 68 ± 3 μm, $n = 105$; ATX+CAT: 63 ± 3 μm, $n = 90$), and they were normalized by vessels cross-sectional areas (mm^2). Each n represents 5.4 ± 0.4 (up to 8) volume acquisitions of an artery of interest and surrounding collateral branches (up to 7) in WT, ATX, and ATX+CAT mice. CBF was reduced in ATX mice, as previously reported (11), and was corrected by CAT ($P < 0.05$) (Fig. 4*B*).

MMP-9 activity in cerebral blood vessels

Pro-MMP-9 activity, the nonactivated form of MMP-9, increased in cerebral vessels from ATX mice (Fig. 5) and was prevented by CAT (Fig. 5). Pro-MMP-2 activity was not detectable (Fig. 5).

VEGF levels

Plasma levels of VEGF were similar in WT and ATX mice; CAT, however, reduced circulating VEGF levels compared with untreated-ATX mice (Fig. 6*A*). In contrast, protein expression of VEGF in mouse cerebral blood vessels was similar between groups (Fig. 6, *B* and *C*).

DISCUSSION

We recently proposed the hypothesis that the endothelium regulates structural and biomechanical properties of cerebral arteries (7). Accordingly, we now report for the first time that, in severely dyslipidemic and moderately hypertensive mice, the preservation of the endothelial function by a chronic treatment with the polyphenol CAT prevented the paradoxical increase in cerebral artery wall compliance, measured both in vitro and in vivo, and impeded the hypertrophic inward remodeling. Importantly, these protective effects of CAT were associated with an improved basal CBF in ATX mice. The combined beneficial effects of CAT on endothelial function, cerebral artery structure, and compliance could, therefore, contribute to the observed maintenance of an adequate cerebral perfusion.

The preventive use of CAT and polyphenols has been shown to improve endothelial function and limit plaque progression by us (11, 16) and others (3, 22, 27). In addition, polyphenols

have been shown to slow the decline in the learning ability associated with brain hypoperfusion (11, 53) and to display neuroprotective effects, partly by preserving endothelial function, possibly through a reduction in lipid peroxidation (19, 20). Whether the prevention of changes in cerebral structural and biomechanical properties, via endothelial preservation, could play a role in the neuroprotective effects of CAT was never tested. Our data suggest that CAT could impede cerebral remodeling and hypoperfusion induced by dyslipidemia indirectly by protecting the endothelial integrity through its anti-oxidant activity: our laboratory previously reported that 3-mo treatment of ATX mice with CAT significantly reduced the abnormal superoxide production in the aorta and cerebral arteries (11). We also reported that CAT increased Mn-super-oxide dismutase expression in the cerebral circulation of the ATX mouse, which could further contribute to the beneficial effect of CAT (11). The antioxidant effect of CAT was associated with the preservation of the endothelial function: indeed, CAT preserved cerebrovascular endothelial nitric oxide synthase (eNOS) activity induced by either acetylcholine or flow, which was decreased in 6-mo ATX mice (7, 11) and nearly abolished at 12 mo of age (12). The endothelial dysfunction in cerebral arteries from ATX mice was characterized by the fact that the lower endothelium-dependent dilations were insensitive to eNOS inhibition; one of the mechanisms by which CAT prevented endothelial dysfunction was by maintaining the sensitivity to eNOS inhibitors (7, 11). In the present study, we demonstrate that CAT also prevents structural and biomechanical alterations in the cerebrovasculature of ATX mice; the combined beneficial effects of CAT on superoxide accumulation in cerebral arteries, eNOS-dependent dilation, and increase in antioxidant enzyme such as Mn-superoxide dismutase, likely protected the cerebral arteries and prevented their remodeling. Altogether, these data suggest that endothelial dysfunction in the cerebrovasculature, related to the prooxidative environment associated with severe dyslipidemia and atherosclerosis, contributes to remodeling, leading ultimately to hypoperfusion.

Oxidative stress-associated inflammation is a known stimulus for arterial wall remodeling (8, 43). A reduction in vascular oxidative stress and global inflammation (evidenced by a reduction in plasma VEGF levels, Fig. 6*A*) could, therefore, prevent the abnormal remodeling of cerebral arteries from ATX mice. ROS production by vascular cells, mainly under the control of NADPH oxidases, is known to trigger vascular smooth muscle cell (VSMC) hyperplasia and/or hypertrophy (33, 50). Very little is known about the involvement of ROS in cerebral artery remodeling associated with atherosclerosis. It was previously reported that treatment of spontaneously hypertensive rats with the O_2^- scavenger Tempol improved the structure of the MCA independently of blood pressure reduction, suggesting as well that ROS contribute to the remodeling of the cerebral vasculature (39). Likewise, in the present study, CAT prevented the reduction of lumen diameter and the thickening of the cerebral arterial wall without reducing blood pressure, suggestive of a free radical-dependent inward hypertrophic remodeling (29) of PCA isolated from ATX mice. These macroscale parameters (lumen diameter, wall thickness, and wall-to-lumen ratio) cannot characterize the cellular and molecular modifications; nonetheless, the inward hypertrophic remodeling implies that there is an increase of material into the arterial wall.

CAT could also prevent cerebral remodeling by inhibiting MMP activity and VSMC proliferation (28, 51), since degradation of the extracellular matrix by MMPs stimulates the migration and proliferation of VSMC and intimal thickening (18, 32). In the context of cerebral ischemia, gelatinases MMP-2, and especially MMP-9, contribute to the pathological process by disturbing the cerebral vasculature integrity, leading to neuroinflammation, brain edema, and hemorrhages (2, 37). In this context, (−)-epigallocatechin gallate has been reported to limit brain infract size and neuronal damage by inhibiting MMP-9 activity (37, 38). In the present study, we demonstrate that MMP-9 activity was significantly higher in cerebral vessels from ATX mice than from WT mice and that a chronic treatment for 3 mo with CAT significantly prevented this rise in MMP-9 activity (Fig. 5). Thus MMP-9 activity was impacted by the long-term treatment with the antioxidant, confirming that ROS trigger MMP-9 activity (54). On the other hand, since it has been reported that CAT could have a direct inhibitory effect on MMP activity (10, 14, 15, 38), we tested the effect of acute addition of CAT directly in the zymography buffer: adding 3.1 μM CAT to cerebrovascular proteins from ATX mice did not acutely reverse the activation of MMP-9 and did not inhibit the activity of recombinant pro-MMP-9 (data not shown). Thus the effects of CAT on MMP-9 activity are not direct, but modulated on the long term and possibly linked to endothelial preservation. There are known interrelationships between cerebrovascular compliance and eNOS (6), and nitric oxide inactivates MMP-9 in peripheral arteries through the MMP-9/nitric oxide/tissue inhibitor of MMP complex (42, 49). The relationship between eNOS and MMP-9 is unknown in cerebral arteries. It is possible, however, that, since CAT preserves cerebral eNOS activity by scavenging ROS, this will result in MMP-9 inactivation and thus changes in wall structure/compliance. This hypothesis remains to be proven, by the use of MMP-9 inhibitor, for example, since doxacyclin prevented the remodeling of the MCA of stroke-prone hypertensive rats (39). Nonetheless, our data reveal that, in a prooxidant and proinflammatory environment, cerebral endothelial dysfunction is associated with MMP-9 activation. Taking into account that mouse cerebral arteries lack external elastica lamina and adventitia (25), such increase in pro-MMP-9 activity would most likely perturb vessel wall extracellular matrix composition and structure, leading to the weakening of the walls. The beneficial antioxidant effects of CAT on eNOS activity revealed by the improved FMD could, therefore, contribute to the reduction of MMP-9 activity observed in this study and, therefore, prevent changes in compliance and in wall remodeling.

In accordance with its protective effect on endothelial function (Fig. 3), structure and biomechanics (Figs. 1, *B* and *D*, 2, and 4*A*), CAT improved basal CBF (Fig. 4*B*). This contrasts with our recent work showing that CAT did not improve the basal cerebral perfusion in 6-mo ATX mice (11). This dissimilarity can be explained by at least two reasons. First, the anesthetic used during basal CBF measurement is different; we changed pentobarbital sodium used in Ref. 11 to urethane to maintain a normal physiological metabolic activity. Indeed, pentobarbital strongly reduces HR (172 ± 4 beats/min compared with 492 ± 5 beats/min with urethane); urethane, therefore, permits to maintain a resting HR similar to that measured in conscious, unrestrained animals [504 ± 15 beats/min (7)]. Second, the present work includes arteries in a larger range of vessel size, by considering an artery and all its collateral branches within 600-μm depth. For these reasons, we would like to propose that we have now optimized the method for the precise measurement of basal

CBF in a single artery. Nonetheless, the improvement in basal CBF observed in this study by CAT could be challenged in conditions needing higher shear stresses, such as during mental and physical exercises. Indeed, in CAT-treated mice, the FMD curve is biphasic, suggesting that the protective effect of CAT is limited and does not allow for an optimal chronic endothelial cell repair and maintenance; this prevents a physiological endothelial response for shear stresses >10 dyn/cm^2 (Fig. 3) and could lead to inadequate cerebral perfusion. This limited effect of CAT contrasts with the preservation of FMD over the whole range of shear stresses obtained after 3 mo of voluntary exercise in ATX mice (Fig. 4C in Ref. 7), suggesting that the long-term outcome of CAT and voluntary exercise on CBF may be different, despite similar beneficial effect of CAT and physical training on cerebral compliance and their absence of effect on carotid stiffness (Fig. 1 and Ref. 7).

There is, however, a limitation to the interpretation of our results of CBF: the large variability in resting HR in WT and ATX mice revealed that resting HR is positively correlated with basal CBF (data not shown). Since blood pressure was not recorded during imaging of the cerebral vessels, the impact of resting HR on blood pressure and CBF will need to be assessed in further studies. In mice, in which resting HR was similar among groups, however, a reduction in basal CBF was observed in ATX mice, and this hypoperfusion was prevented by CAT treatment.

Why, however, do cerebral and carotid arteries from ATX mice display opposite changes in vascular compliance? ATX mice are slightly hypertensive (7), and atherosclerotic plaques develop in the aorta, the renal arteries, the carotids, but not in the cerebral arteries (11, 16). Carotid plaque is associated with carotid stiffening, and this likely lowers the “buffering” capacity of the carotids, promoting the propagation of the pulse pressure to small vessels in the brain (34). Since cerebral arteries lack external elastic lamina and adventitia (24), these hemodynamic changes would likely be sufficient to weaken the wall of the cerebral arteries. In addition, the changes associated with atherosclerosis in the composition or in the organization of structural elastin and collagen fibers are likely to have more impact in the mechanical properties of conductance arteries, such as carotids, than in cerebral arteries (5). We believe, however, that the fundamental difference between carotid and cerebral changes in compliance resides in the relative role of the endothelium and their sensitivity to biomechanical stress: the carotid artery wall is directly exposed to the mechanical stress. Thus carotid stiffness can be prevented by reducing HR, for example, with the pacemaker current inhibitor ivabradine or the β-blocker metoprolol (7). In contrast, in cerebral arteries that develop myogenic responses and are less exposed to mechanical stress, compliance is mostly regulated by the endothelium: the better the endothelial function, the lower the cerebrovascular compliance (7). The mechanical stress only amplifies cerebral endothelial dysfunction, favoring remodeling. Accordingly, we demonstrate in the present study that CAT preserves both cerebral endothelial function and compliance, while carotid stiffness is not improved. The endothelium is, therefore, a key player regulating the cerebrovascular, but not carotid, biomechanical properties. To the best of our knowledge, a direct endothelium-dependent regulation of cerebrovascular compliance has never been reported. Because the increase in compliance and endothelial dysfunction we observed were triggered by a chronic exposition of cerebral vessels to the pathological environment created by atherosclerosis, only indirect evidence can be provided.

In conclusion, our results extend from our laboratory's previous studies (7, 11) by demonstrating that preservation of the endothelial function by CAT improves cerebrovascular wall biomechanics. The mechanism of action of CAT likely involves a reduction in cerebral ROS availability, preserving eNOS, which subsequently could reduce MMP-9 activity and prevent the changes in structure and compliance. These combined effects lead to an improved basal CBF. Therefore, the observed preservation of cognitive function by CAT in ATX mice (11) goes beyond the sole improvement of the endothelial function. It demonstrates that the cerebral artery wall is an integrated system, and that strategies aiming at preventing cerebrovascular dysfunction and the associated cognitive decline will likely need to integrate biomechanics as a determinant functional parameter.

Acknowledgments

GRANTS

This work has been supported in part by the Montreal Heart Institute Foundation, the Heart and Stroke Foundation of Quebec, and the Canadian Institutes of Health Research (MOP89733).

References

1. Albaladejo P, Carusi A, Apartian A, Lacolley P, Safar ME, Benetos A. Effect of chronic heart rate reduction with ivabradine on carotid and aortic structure and function in normotensive and hypertensive rats. J Vasc Res. 2003; 40:320–328. [PubMed: 12891001]
2. Asahi M, Wang X, Mori T, Sumii T, Jung JC, Moskowitz MA, Fini ME, Lo EH. Effects of matrix metalloproteinase-9 gene knock-out on the proteolysis of blood-brain barrier and white matter components after cerebral ischemia. J Neurosci. 2001; 21:7724–7732. [PubMed: 11567062]
3. Auclair S, Milenkovic D, Besson C, Chauvet S, Gueux E, Morand C, Mazur A, Scalbert A. Catechin reduces atherosclerotic lesion development in apo E-deficient mice: a transcriptomic study. Atherosclerosis. 2009; 204:e21–e27. [PubMed: 19152914]
4. Baraghis E, Bolduc V, Lefebvre J, Srinivasan VJ, Boudoux C, Thorin E, Lesage F. Measurement of cerebral microvascular compliance in a model of atherosclerosis with optical coherence tomography. Biomedical Opt Express. 2011; 2:3079–3093.
5. Baumbach GL, Sigmund CD, Faraci FM. Cerebral arteriolar structure in mice overexpressing human renin and angiotensinogen. Hypertension. 2003; 41:50–55. [PubMed: 12511529]
6. Baumbach GL, Sigmund CD, Faraci FM. Structure of cerebral arterioles in mice deficient in expression of the gene for endothelial nitric oxide synthase. Circ Res. 2004; 95:822–829. [PubMed: 15388643]
7. Bolduc V, Drouin A, Gillis MA, Duquette N, Thorin-Trescases N, Frayne-Robillard I, Des Rosiers C, Tardif JC, Thorin E. Heart rate-associated mechanical stress impairs carotid but not cerebral artery compliance in dyslipidemic atherosclerotic mice. Am J Physiol Heart Circ Physiol. 2011; 301:H2081–H2092. [PubMed: 21926346]
8. Chatzizisis YS, Giannoglou GD. Coronary hemodynamics and atherosclerotic wall stiffness: a vicious cycle. Med Hypotheses. 2007; 69:349–355. [PubMed: 17343988]
9. Chyu KY, Babbidge SM, Zhao X, Dandillaya R, Rietveld AG, Yano J, Dimayuga P, Cercek B, Shah PK. Differential effects of green tea-derived catechin on developing versus established atherosclerosis in apo-lipoprotein E-null mice. Circulation. 2004; 109:2448–2453. [PubMed: 15136500]
10. Demeule M, Brossard M, Page M, Gingras D, Beliveau R. Matrix metalloproteinase inhibition by green tea catechins. Biochim Biophys Acta. 2000; 1478:51–60. [PubMed: 10719174]
11. Drouin A, Bolduc V, Thorin-Trescases N, Belanger E, Fernandes P, Baraghis E, Lesage F, Gillis MA, Villeneuve L, Hamel E, Ferland G, Thorin E. Catechin treatment improves cerebrovascular flow-mediated dilation and learning abilities in atherosclerotic mice. Am J Physiol Heart Circ Physiol. 2011; 300:H1032–H1043. [PubMed: 21186270]

12. Drouin A, Farhat N, Bolduc V, Thorin-Trescases N, Gillis MA, Villeneuve L, Nguyen A, Thorin E. Up-regulation of thromboxane A impairs cerebrovascular eNOS function in aging atherosclerotic mice. Pflügers Arch. 2011; 462:371–383. [PubMed: 21617900]
13. Drouin A, Thorin E. Flow-induced dilation is mediated by Akt-dependent activation of endothelial nitric oxide synthase-derived hydrogen peroxide in mouse cerebral arteries. Stroke. 2009; 40:1827–1833. [PubMed: 19286591]
14. Garbisa S, Biggin S, Cavallarin N, Sartor L, Benelli R, Albini A. Tumor invasion: molecular shears blunted by green tea. Nat Med. 1999; 5:1216. [PubMed: 10545959]
15. Garbisa S, Sartor L, Biggin S, Salvato B, Benelli R, Albini A. Tumor gelatinases and invasion inhibited by the green tea flavanol epigallocatechin-3-gallate. Cancer. 2001; 91:822–832. [PubMed: 11241252]
16. Gendron ME, Theoret JF, Mamarbachi AM, Drouin A, Nguyen A, Bolduc V, Thorin-Trescases N, Merhi Y, Thorin E. Late chronic catechin antioxidant treatment is deleterious to the endothelial function in aging mice with established atherosclerosis. Am J Physiol Heart Circ Physiol. 2010; 298:H2062–H2070. [PubMed: 20382853]
17. Giannattasio C, Vincenti A, Failla M, Capra A, Ciro A, De Ceglia S, Gentile G, Brambilla R, Mancia G. Effects of heart rate changes on arterial distensibility in humans. Hypertension. 2003; 42:253–256. [PubMed: 12913054]
18. Gurjar MV, Sharma RV, Bhalla RC. eNOS gene transfer inhibits smooth muscle cell migration and MMP-2 and MMP-9 activity. Arterioscler Thromb Vasc Biol. 1999; 19:2871–2877. [PubMed: 10591663]
19. Haque AM, Hashimoto M, Katakura M, Tanabe Y, Hara Y, Shido O. Long-term administration of green tea catechins improves spatial cognition learning ability in rats. J Nutr. 2006; 136:1043–1047. [PubMed: 16549472]
20. Hong JT, Ryu SR, Kim HJ, Lee JK, Lee SH, Kim DB, Yun YP, Ryu JH, Lee BM, Kim PY. Neuroprotective effect of green tea extract in experimental ischemia-reperfusion brain injury. Brain Res Bull. 2000; 53:743–749. [PubMed: 11179838]
21. Judkins CP, Diep H, Broughton BR, Mast AE, Hooker EU, Miller AA, Selemidis S, Dusting GJ, Sobey CG, Drummond GR. Direct evidence of a role for Nox2 in superoxide production, reduced nitric oxide bioavailability, and early atherosclerotic plaque formation in ApoE−/− mice. Am J Physiol Heart Circ Physiol. 2010; 298:H24–H32. [PubMed: 19837950]
22. Kaliora AC, Dedoussis GV, Schmidt H. Dietary antioxidants in preventing atherogenesis. Atherosclerosis. 2006; 187:1–17. [PubMed: 16313912]
23. Kleiner DE, Stetler-Stevenson WG. Quantitative zymography: detection of picogram quantities of gelatinases. Anal Biochem. 1994; 218:325–329. [PubMed: 8074288]
24. Lee HY, Oh BH. Aging and arterial stiffness. Circ J. 2010; 74:2257–2262. [PubMed: 20962429]
25. Lee RM. Morphology of cerebral arteries. Pharmacol Ther. 1995; 66:149–173. [PubMed: 7630927]
26. Li X, Geary GG, Gonzales RJ, Krause DN, Duckles SP. Effect of estrogen on cerebrovascular prostaglandins is amplified in mice with dysfunctional NOS. Am J Physiol Heart Circ Physiol. 2004; 287:H588–H594. [PubMed: 15277199]
27. Loke WM, Proudfoot JM, Hodgson JM, McKinley AJ, Hime N, Magat M, Stocker R, Croft KD. Specific dietary polyphenols attenuate atherosclerosis in apolipoprotein E-knockout mice by alleviating inflammation and endothelial dysfunction. Arterioscler Thromb Vasc Biol. 2010; 30:749–757. [PubMed: 20093625]
28. Lu LH, Lee SS, Huang HC. Epigallocatechin suppression of proliferation of vascular smooth muscle cells: correlation with c-jun and JNK. Br J Pharmacol. 1998; 124:1227–1237. [PubMed: 9720795]
29. Martinez-Lemus LA, Hill MA, Meininger GA. The plastic nature of the vascular wall: a continuum of remodeling events contributing to control of arteriolar diameter and structure. Physiology (Bethesda). 2009; 24:45–57. [PubMed: 19196651]
30. Mircoli L, Mangoni AA, Giannattasio C, Mancia G, Ferrari AU. Heart rate-dependent stiffening of large arteries in intact and sympathectomized rats. Hypertension. 1999; 34:598–602. [PubMed: 10523333]

31. Muller JM, Davis MJ, Chilian WM. Integrated regulation of pressure and flow in the coronary microcirculation. Cardiovasc Res. 1996; 32:668–678. [PubMed: 8915185]
32. Newby AC. Matrix metalloproteinases regulate migration, proliferation, and death of vascular smooth muscle cells by degrading matrix and non-matrix substrates. Cardiovasc Res. 2006; 69:614–624. [PubMed: 16266693]
33. Niu XL, Madamanchi NR, Vendrov AE, Tchivilev I, Rojas M, Madamanchi C, Brandes RP, Krause KH, Humphries J, Smith A, Burnand KG, Runge MS. Nox activator 1: a potential target for modulation of vascular reactive oxygen species in atherosclerotic arteries. Circulation. 2010; 121:549–559. [PubMed: 20083677]
34. O'Rourke MF, Hashimoto J. Mechanical factors in arterial aging: a clinical perspective. J Am Coll Cardiol. 2007; 50:1–13. [PubMed: 17601538]
35. Okuyama S, Okuyama J, Tamatsu Y, Shimada K, Hoshi H, Iwai J. The arterial circle of Willis of the mouse helps to decipher secrets of cerebral vascular accidents in the human. Med Hypotheses. 2004; 63:997–1009. [PubMed: 15504567]
36. Papaioannou TG, Karatzis EN, Vavuranakis M, Lekakis JP, Stefanadis C. Assessment of vascular wall shear stress and implications for atherosclerotic disease. Int J Cardiol. 2006; 113:12–18. [PubMed: 16889847]
37. Park JW, Hong JS, Lee KS, Kim HY, Lee JJ, Lee SR. Green tea polyphenol(−)-epigallocatechin gallate reduces matrix metalloproteinase-9 activity following transient focal cerebral ischemia. J Nutr Biochem. 2010; 21:1038–1044. [PubMed: 19962294]
38. Park JW, Jang YH, Kim JM, Lee H, Park WK, Lim MB, Chu YK, Lo EH, Lee SR. Green tea polyphenol(−)-epigallocatechin gallate reduces neuronal cell damage and up-regulation of MMP-9 activity in hippocampal CA1 and CA2 areas following transient global cerebral ischemia. J Neurosci Res. 2009; 87:567–575. [PubMed: 18752302]
39. Pires PW, Deutsch C, McClain JL, Rogers CT, Dorrance AM. Tempol, a superoxide dismutase mimetic, prevents cerebral vessel remodeling in hypertensive rats. Microvasc Res. 2010; 80:445–452. [PubMed: 20600163]
40. Pries AR, Neuhaus D, Gaehtgens P. Blood viscosity in tube flow: dependence on diameter and hematocrit. Am J Physiol Heart Circ Physiol. 1992; 263:H1770–H1778.
41. Sanan DA, Newland DL, Tao R, Marcovina S, Wang J, Mooser V, Hammer RE, Hobbs HH. Low density lipoprotein receptor-negative mice expressing human apolipoprotein B-100 develop complex atherosclerotic lesions on a chow diet: no accentuation by apolipoprotein(a). Proc Natl Acad Sci U S A. 1998; 95:4544–4549. [PubMed: 9539774]
42. Steed MM, Tyagi N, Sen U, Schuschke DA, Joshua IG, Tyagi SC. Functional consequences of the collagen/elastin switch in vascular remodeling in hyperhomocysteinemic wild-type, eNOS−/−, and iNOS−/− mice. Am J Physiol Lung Cell Mol Physiol. 2010; 299:L301–L311. [PubMed: 20581102]
43. Sugawara J, Komine H, Hayashi K, Yoshizawa M, Yokoi T, Otsuki T, Shimojo N, Miyauchi T, Maeda S, Tanaka H. Effect of systemic nitric oxide synthase inhibition on arterial stiffness in humans. Hypertens Res. 2007; 30:411–415. [PubMed: 17587753]
44. Sutherland BA, Shaw OM, Clarkson AN, Jackson DN, Sammut IA, Appleton I. Neuroprotective effects of (−)-epigallocatechin gallate following hypoxia-ischemia-induced brain damage: novel mechanisms of action. FASEB J. 2005; 19:258–260. [PubMed: 15569775]
45. Tanabe N, Suzuki H, Aizawa Y, Seki N. Consumption of green and roasted teas and the risk of stroke incidence: results from the Tokamachi-Nakasato cohort study in Japan. Int J Epidemiol. 2008; 37:1030–1040. [PubMed: 18832387]
46. Tonstad S, Joakimsen O, Stensland-Bugge E, Ose L, Bonaa KH, Leren TP. Carotid intima-media thickness and plaque in patients with familial hypercholesterolaemia mutations and control subjects. Eur J Clin Invest. 1998; 28:971–979. [PubMed: 9893006]
47. Touboul PJ, Labreuche J, Vicaut E, Amarenco P. Carotid intima-media thickness, plaques, and Framingham risk score as independent determinants of stroke risk. Stroke. 2005; 36:1741–1745. [PubMed: 16020769]

48. Tournaire C, Croux S, Maurette MT, Beck I, Hocquaux M, Braun AM, Oliveros E. Antioxidant activity of flavonoids: efficiency of singlet oxygen (1 delta g) quenching. J Photochem Photobiol B. 1993; 19:205–215. [PubMed: 8229463]
49. Tronc F, Mallat Z, Lehoux S, Wassef M, Esposito B, Tedgui A. Role of matrix metalloproteinases in blood flow-induced arterial enlargement: interaction with NO. Arterioscler Thromb Vasc Biol. 2000; 20:E120–E126. [PubMed: 11116076]
50. Ushio-Fukai M, Zafari AM, Fukui T, Ishizaka N, Griendling KK. p22phox is a critical component of the superoxidegenerating NADH/NADPH oxidase system and regulates angiotensin II-induced hypertrophy in vascular smooth muscle cells. J Biol Chem. 1996; 271:23317–23321. [PubMed: 8798532]
51. Won SM, Park YH, Kim HJ, Park KM, Lee WJ. Catechins inhibit angiotensin II-induced vascular smooth muscle cell proliferation via mitogen-activated protein kinase pathway. Exp Mol Med. 2006; 38:525–534. [PubMed: 17079869]
52. Xie C, Kang J, Burris R, Ferguson ME, Schauss AG, Nagarajan S, Wu X. Acai juice attenuates atherosclerosis in ApoE deficient mice through antioxidant and anti-inflammatory activities. Atherosclerosis. 2011; 216:327–333. [PubMed: 21411096]
53. Xu Y, Zhang JJ, Xiong L, Zhang L, Sun D, Liu H. Green tea polyphenols inhibit cognitive impairment induced by chronic cerebral hypoperfusion via modulating oxidative stress. J Nutr Biochem. 2010; 21:741–748. [PubMed: 19615878]
54. Zalba G, Fortuno A, Orbe J, San Jose G, Moreno MU, Belzunce M, Rodriguez JA, Beloqui O, Paramo JA, Diez J. Phagocytic NADPH oxidase-dependent superoxide production stimulates matrix metalloproteinase-9: implications for human atherosclerosis. Arterioscler Thromb Vasc Biol. 2007; 27:587–593. [PubMed: 17194891]

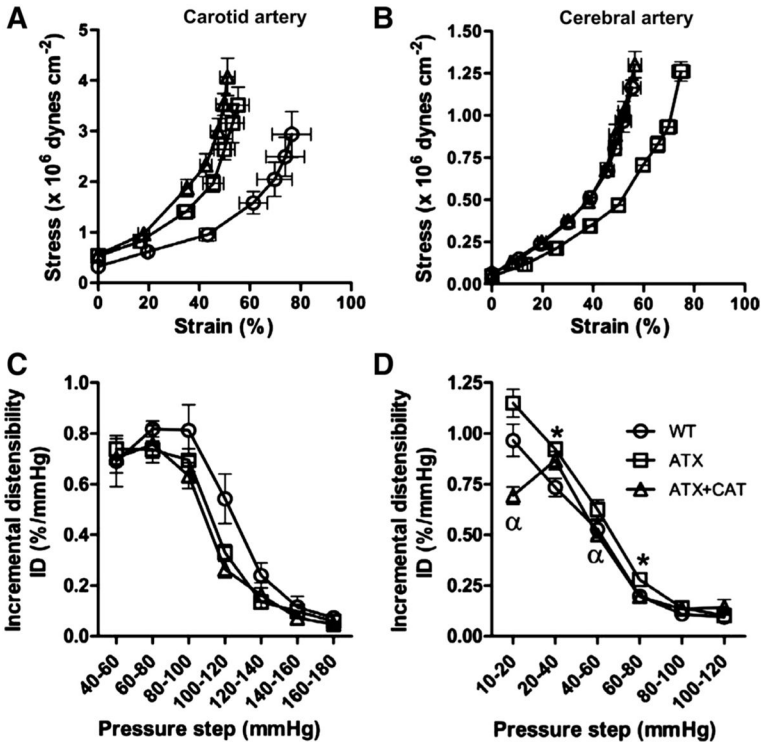

Fig. 1.

Effect of a chronic treatment with (+)-catechin (CAT) of 6-mo LDLr$^{-/-}$:hApoB$^{+/+}$ [atherosclerotic (ATX)] mice, on the arterial compliance expressed as the stress-strain relationship (*A* and *B*) and on the distensibility expressed as incremental distensibility (ID; %/mmHg; *C* and *D*) in carotid arteries (*A* and *C*) and cerebral arteries (*B* and *D*). Values are means ± SE of 5–9 mice for carotid arteries and of 10 –17 mice for cerebral arteries. WT, wild type. **P* < 0.05 vs. WT mice. **P* < 0.05 vs. ATX mice.

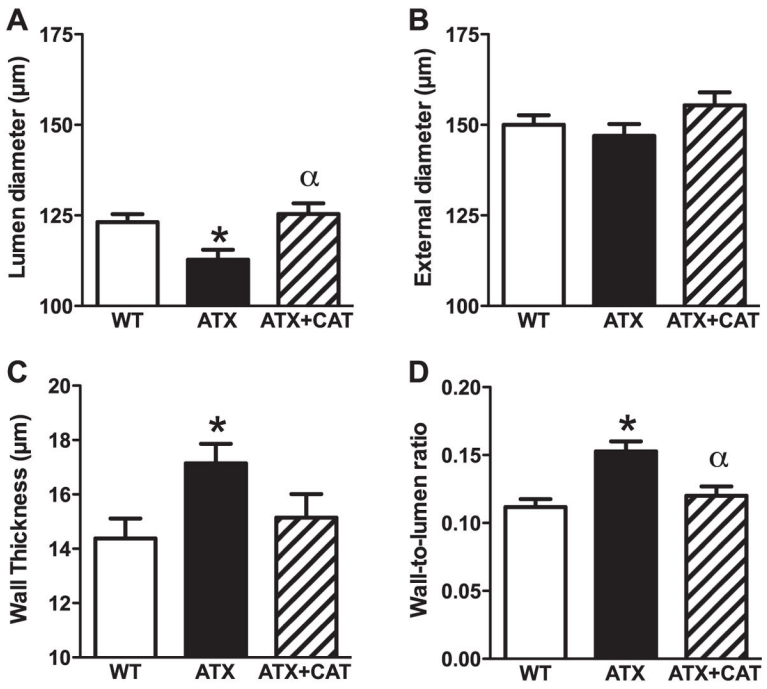

Fig. 2.

Effect of a chronic treatment with CAT of 6-mo LDLr$^{-/-}$:hApoB$^{+/+}$ (ATX) mice, on the structural changes occurring in cerebral arteries. *A*: vessel lumen diameter; *B*: vessel external diameter; *C*: vessel wall thickness; *D*: wall-to-lumen ratio. Values are means ± SE of 10 –17 mice. *$P < 0.05$ vs. WT mice. $^{\alpha}P < 0.05$ vs. ATX mice.

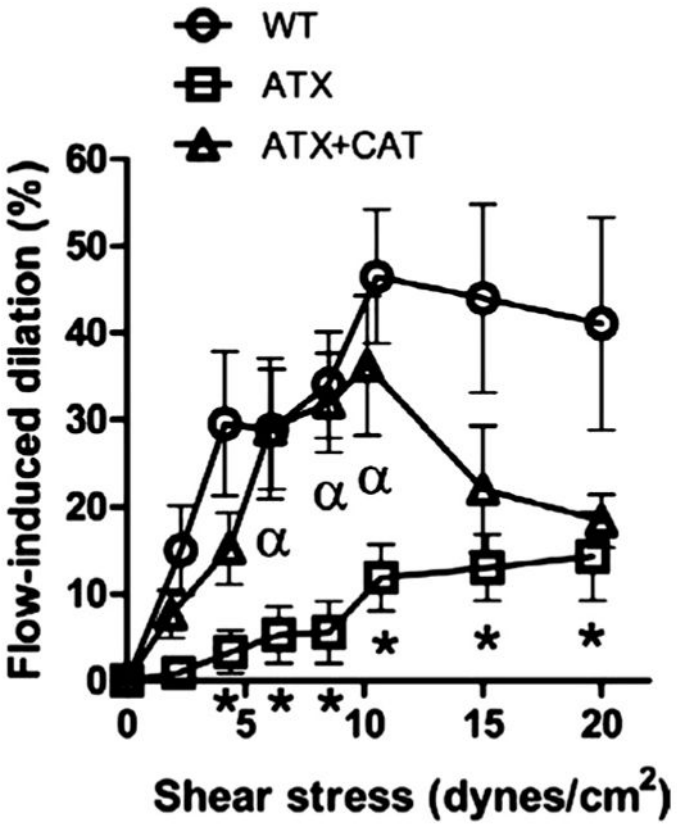

Fig. 3.

Effect of chronic treatment with CAT of 6-mo LDLr$^{-/-}$:hApoB$^{+/+}$ (ATX) mice, on flow-mediated endothelium-dependent dilations induced by increasing shear stresses (dyn/cm^2) of pressurized cerebral arteries. Values are means ± SE of 10 –17 mice. *$P < 0.05$ vs. WT mice. $^{\alpha}P < 0.05$ vs. ATX mice.

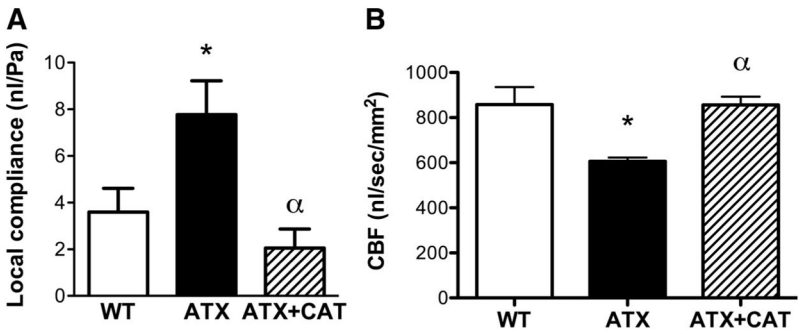

Fig. 4.

Effect of a chronic treatment with CAT of 6-mo LDLr$^{-/-}$:hApoB$^{+/+}$ (ATX) mice on in vivo cerebral compliance expressed as the local compliance evaluator (nl/Pa) (*A*) and basal cerebral blood flow (CBF; nl/s) normalized to arterial area (mm^2) and evaluated in the microvasculature (*B*). *A*: values are means ± SE of 10 mice for WT and ATX mice and of 4 mice for ATX+CAT mice. *B*: values are means ± SE of 78 vessels for WT mice, 25 for ATX mice, and 88 for ATX+CAT mice. *$P < 0.05$ vs. WT mice. $^{\alpha}P < 0.05$ vs. ATX mice.

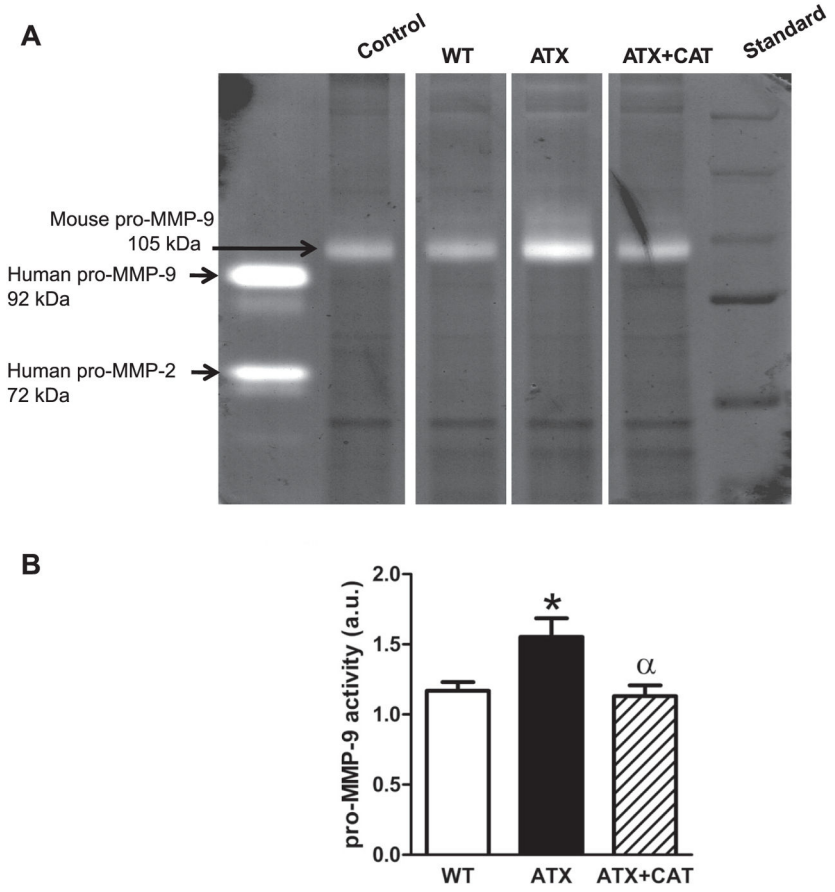

Fig. 5.

A: representative example of zymography illustrating pro-matrix metalloproteinase (MMP)-9 activities of cerebral vessels from WT, $LDLr^{-/-}$: $hApoB^{+/+}$ (ATX) mice, and ATX treated with CAT. *B*: each set of experiment was normalized to a reference sample (loaded in every experiments). Values are means ± SE of 6 mice. au, Arbitrary units. $^{*}P < 0.05$ vs. WT mice. $^{\alpha}P < 0.05$ vs. ATX mice.

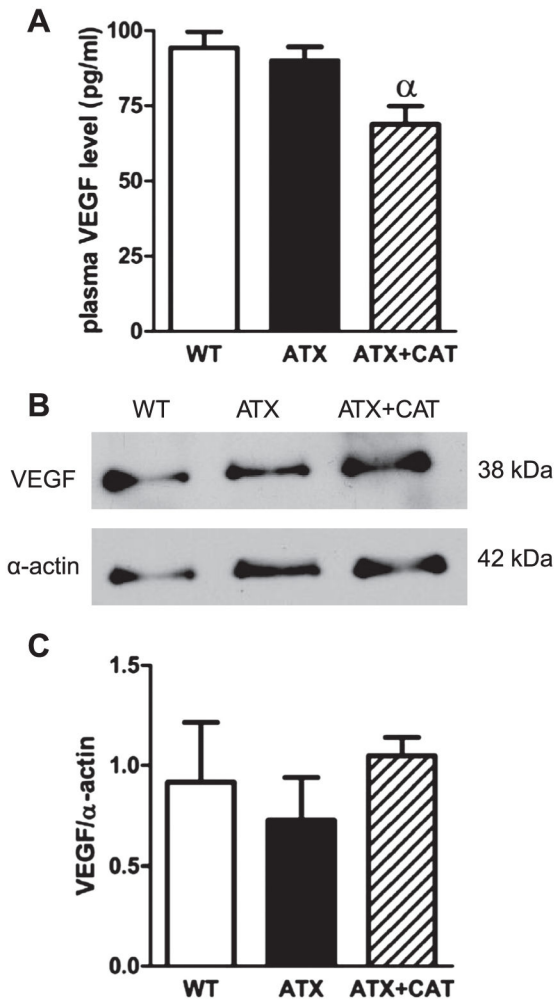

Fig. 6.

A: effect of a chronic treatment of 6-mo LDLr$^{-/-}$:hApoB$^{+/+}$ (ATX) mice with CAT on plasma VEGF level. *B*: representative example of Western blot illustrating VEGF protein expression of total cerebral vessels from WT and ATX mice treated, or not, with CAT. *C*: graph represents the protein expression normalized to a reference sample (loaded in every experiment) and after normalization with smooth muscle α-actin. Values are means ± SE of 4 –5 mice. $^{\alpha}P < 0.05$ vs. ATX mice.

Table 1

Body weight, plasma lipids, and glucose levels in mice

Mice	Weight, g	Total Cholesterol, mM	LDL-Cholesterol, mM	HDL-Cholesterol, mM	TG, mM	Glucose, mM
6-mo WT	36 ± 1 (13)	2.1 ± 0.2 (5)	0.7 ± 0.1 (5)	1.2 ± 0.1 (5)	0.7 ± 0.1 (5)	26.8 ± 3.0 (5)
6-mo ATX	32 ± 2 (12)	15.7 ± 1.3*(5)	10.3 ± 1.2*(5)	1.6 ± 0.1*(5)	7.2 ± 1.3*(5)	15.9 ± 3.6*(5)
6-mo ATX + CAT	31 ± 1 (10)	22.3 ± 1.3†(5)	15.0 ± 1.1†(5)	1.6 ± 0.1 (5)	6.5 ± 0.6 (5)	19.8 ± 1.5 (5)

Values are means ± SE; *n*, no. of mice are in parentheses. WT, wild-type mice; ATX, atherosclerotic, LDLr$^{-/-}$:hApoB$^{+/+}$ mice; ATX+ CAT, LDLr$^{-/-}$:hApoB$^{+/+}$ mice treated with (+)-catechin (CAT; 30 mg · kg^{-1} · day^{-1}); LDL, low-density lipoprotein; HDL, high-density lipoprotein; TG, triglycerides.

$^{*}P < 0.05$ vs. 6-mo WT.

$^{\dagger}P < 0.05$ vs. 6-mo ATX.

Table 2

Evolution of heart rate, systolic blood pressure, diastolic blood pressure, and pulse pressure measured by tail cuff in mice during 3 mo of catechin treatment

Mice	*n*	HR, beats/min	SBP, mmHg	DBP, mmHg	PP, mmHg
3-mo WT	6	691 ± 9	137 ± 6	106 ± 5	31 ± 2
6-mo WT	6	684 ± 9	127 ± 3	97 ± 2	30 ± 2
3-mo ATX	11	644 ± 26	146 ± 3	114 ± 3	32 ± 1
6-mo ATX	5	662 ± 18	146 ± 7*	112 ± 6*	34 ± 2
6-mo ATX + CAT	6	602 ± 23	141 ± 8	108 ± 7	33 ± 1

Values are means ± SE; *n*, no. of mice. HR, heart rate; SBP, systolic blood pressure; DBP, diastolic blood pressure; PP, pulse pressure.

*$P < 0.05$ vs. 6-mo WT.